JOURNAL OF MATERIALS SCIENCE 35 (2000) 2079–2086

Microdeformation of a polydomain, smectic liquid crystalline thermoset

C. ORTIZ*, L. BELENKY, C. K. OBER, E. J. KRAMER‡
Cornell University, Department of Materials Science and Engineering and The Materials Science Center, Bard Hall, Ithaca, NY 14850, USA
E-mail: cober@msc.cornell.edu

The microdeformation and fracture mechanisms of a densely crosslinked, polydomain, smectic liquid crystalline thermoset (LCT) were investigated in order to gain some insight into its interesting mechanical properties (e.g. improved fracture toughness). A difunctional LC epoxy monomer, diglycidyl ether of 4,4′-dihydroxy-α-methylstilbene (DGDHMS), was crosslinked with the tetrafunctional, aromatic crosslinker, 4,4′-methylene dianiline (MDA) to produce the LCT. Thermoset films (30 μm in thickness) were bonded to copper grids, strained in tension, and observed under the polarizing optical microscope. A new type of microdeformation and fracture mechanism was observed for the smectic LCT. At small strains, numerous microcracks formed which were oriented at various angles to the straining direction. Many smaller isolated and interconnected defects (of the order of a single LC domain, $\sim$1 μm in size) surrounded and emanated from the crack tips. At larger strains, the microcracks propagated slowly and stably until reaching a critical size of $\sim$250 μm, at which time they began to widen and change direction, indicative of plastic deformation which extended over many LC domains. Film failure occurred through microcrack interconnection. A fracture mechanism for the LCT is proposed based on microscopic voiding near the crack tip through the failure of individual LC domains.

1. Introduction

Liquid crystalline thermosets (LCT's) are a new class of densely crosslinked network materials that have unusual dynamic mechanical, compressive, and fracture properties [1–14] due to their unique fine-scaled, macroscopically isotropic "polydomain" microstructure [14, 15]. The nature of this microstructure is described in detail in another paper [14] and reviewed briefly in Table I. [14, 16–23] and Fig. 1. In general, the LCT's employed in this study exhibit a Schlieren texture (when viewed under the polarizing optical microscope) with a high disclination density and an average LC domain size (≈average distance between disclinations) of approximately 1 μm (Fig. 1a). Within a single LC domain, the molecules were ordered locally into a smectic phase (Fig. 1b).

As for the case of conventional, amorphous thermosets, LCT's are glassy (Tg $\approx 150^{\circ}$C) and stiff ($E \approx 10^9$ Pa) at room temperature. In addition, the material no longer exhibits liquid crystalline phase transitions; even above Tg, the microstructure and local order of the liquid crystalline phase are permanently "locked into the network. It has been shown that smectic LCT's exhibit exceptionally high fracture toughness (i.e. $G_{Ic} = 1.62\ \mathrm{kJ/m^2}$, $K_{Ic} = 1.59\ \mathrm{MPa{\cdot}m^{1/2}}$ [14]) compared to amorphous, non-LC thermosets (i.e. $G_{Ic} \approx 0.4\ \mathrm{kJ/m^2}$, $K_{Ic} = 1.21\ \mathrm{MPa{\cdot}m^{1/2}}$ [24–27]). Using the chevron-notched three-point bend technique, we have reported [14] that smectic LCT's exhibit slow, stable crack propagation (Fig. 2a), rather than the unstable, catastrophic, brittle failure typically observed in amorphous, non-LC thermosets. SEM analysis of the smectic LCT samples showed extremely deformed, fibrillar fracture surfaces indicative of bulk plastic deformation (Fig. 2b). In order to gain a better understanding of the microscopic deformation mechanisms responsible for the increased macroscopic plastic deformation and fracture toughness of these materials, straining experiments were performed under the polarizing optical microscope on thin films using the copper grid technique developed by Lauterwasser and Kramer [28]. This technique has been applied successfully to study crazing and shear deformation zones in glassy polymers [28–37], microdeformation of polymer blends [38], and more recently, polymer nanofoams [39].

2. Experimental

2.1. Materials

The chemical structures of the materials employed in this study are given in Fig. 3. The liquid crystalline

* *Present Address*: Massachusetts Institute of Technology, Department of Material Science and Engineering, Room 13-4022, 77 Massachusetts Avenue, Cambridge, MA 02139 USA.
‡ *Present Address*: Materials Department, University of Santa Barbara, Santa Barbara, CA 93106-5050, USA.

TABLE I Relevant terminology in describing the microstructure of the liquid crystalline thermosets investigated in this study [16–23]

Term	Definition
Single LC domain	region of uniform molecular orientation
Polydomain microstructure	an assembly of misoriented LC domains
Local director	unit vector, $\hat{n}$, along which the molecules in a single LC domain are oriented
Schlieren texture	nonuniformity of $\hat{n}$ resulting in a field of wavy, dark brushes when viewed under the polarizing optical microscope (the brushes are where $\hat{n}$ is parallel or perpendicular to the polarizer or analyzer axes)
Disclination	a line defect corresponding to an orientational discontinuity in $\hat{n}$, located at the center of the dark rushes in a Schlieren texture
Smectic phase	the molecular long axes are parallel in addition to layering of the molecular centers of gravity into planes or sheets

epoxy monomer used in this study, diglycidyl ether of 4,4′-dihydroxy-α-methylstilbene (DGDHMS), was synthesized according to [15]. Characterization was accomplished by thin layer chromatography (TLC), Fourier transform infrared spectroscopy (Nicolet FTIR/44), and nuclear magnetic resonance (Varian XL-200 ^{1}H NMR). A commercial, non-LC, epoxy monomer of similar molecular weight, diglycidyl ether of bisphenol A (DGEBA), was obtained from the Dow Chemical Co. (DER 332). The crosslinking agent, an aromatic tetrafunctional diamine, 4,4′-methylene dianiline (MDA), was obtained from Aldrich Chemical Co. and used without further purification (purity > 98%). Differential scanning calorimetry (Dupont 2000 DSC cell, heating/cooling rate = 20 °C/min) and the polarizing optical microscope, POM, (Leitz, Inc.) were used in conjunction with a programmable hot stage (Mettler FP-82T, heating/cooling rate = 20 °C/min) to

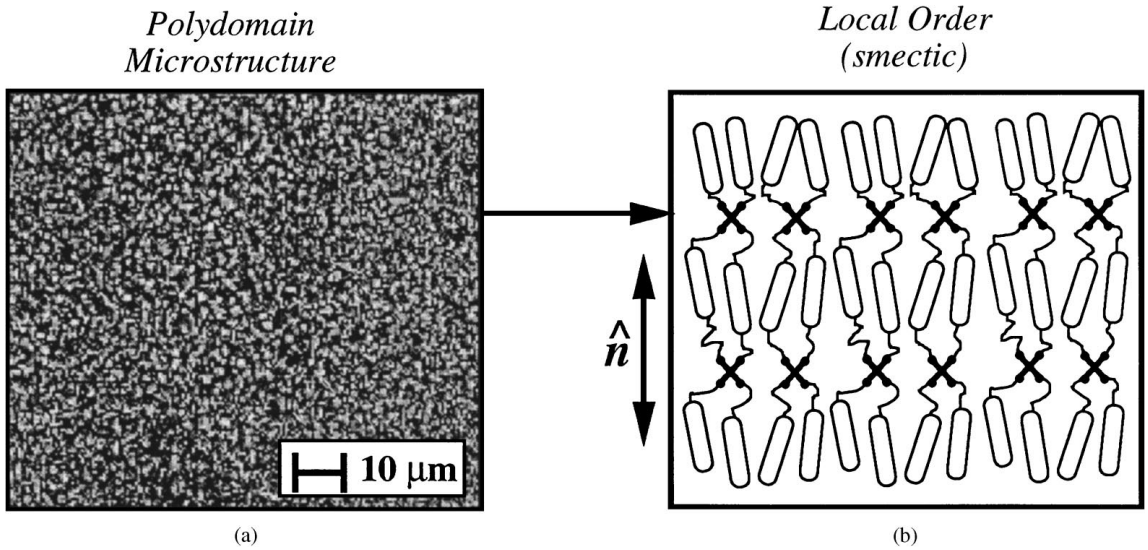

Figure 1 A liquid crystalline thermoset with a (a) macroscopically isotropic, fine-scaled, Schlieren, polydomain microstructure (as viewed under the polarizing optical microscope) and (b) smectic-type local ordering.

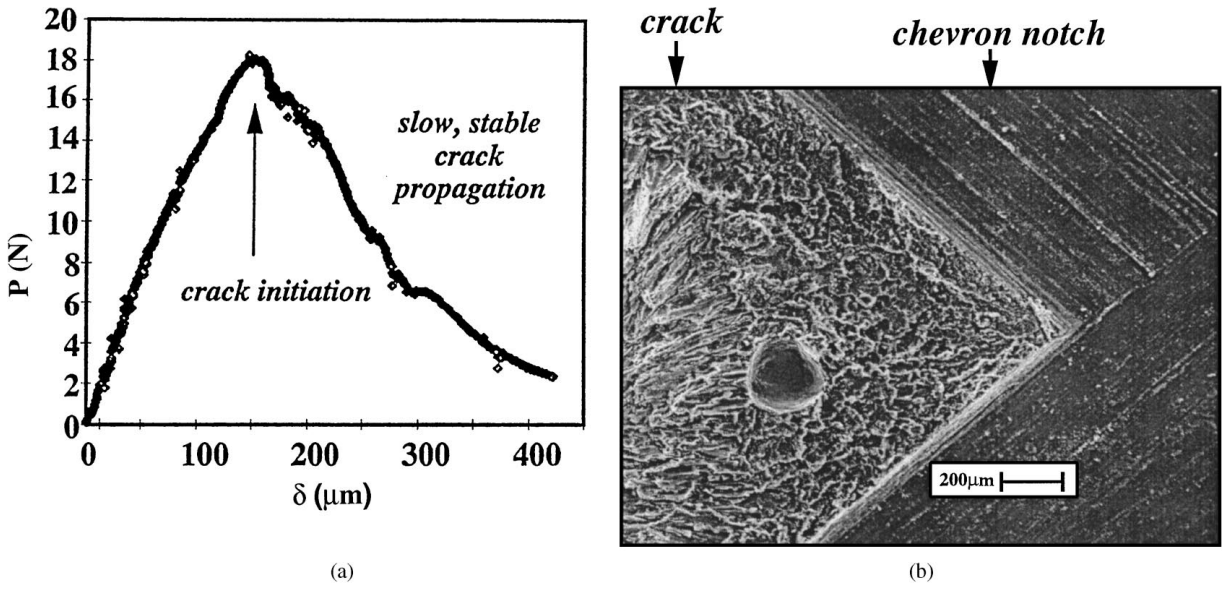

Figure 2 (a) Force versus displacement curve for smectic LCT tested in chevron-notched three-point bend fracture toughness technique and (b) scanning electron micrographs of cross-sectional fracture [14].

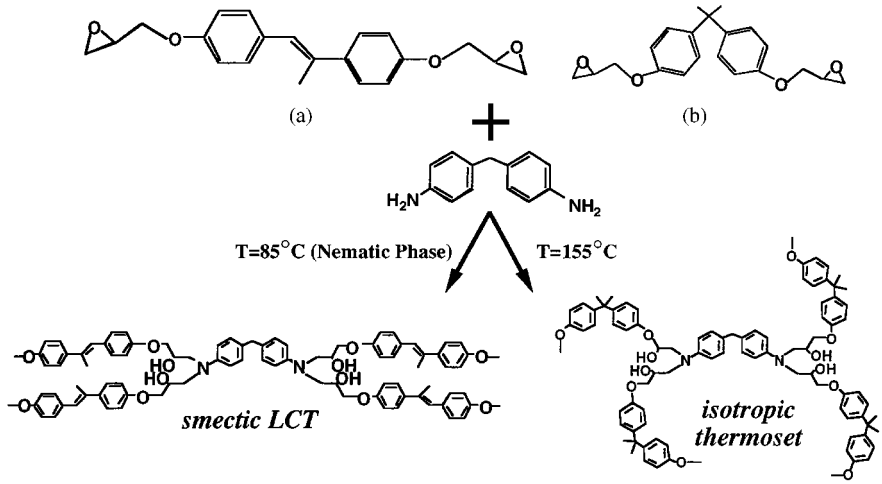

Figure 3 Reaction of the (a) DGDHMS LC monomer or the (b) DGEBA non-LC monomer with the non-LC crosslinker MDA to form a smectic LCT or an amorphous, non-LC thermoset.

characterize thermal transition temperatures of the monomers and stoichiometric epoxy/amine mixtures. The crosslinking reaction takes place as shown in Fig. 3 and is described elsewhere [14].

2.2. Curing and sample preparation

Stoichiometric proportions of epoxy and amine were mechanically ground up with a mortar and pestal. To prepare a sample, 0.1 g of the mixture was sandwiched between a polished sodium chloride disk (diameter = 25 mm, thickness = 4 mm) and an untreated glass slide. In order to produce polydomain, smectic networks, the curing procedure for the DGDHMS/MDA system was carried out as follows according to the time-temperature-LC transformation diagram reported in [14]. The epoxy/amine mixture was first heated above its melting point (≈150°C) in order to form an isotropic, uniform polymer film. The film was then brought to 85°C (i.e. within the LC phase of the mixture) within 1 minute where isothermal curing was carried out for 3 hours. The DGEBA/MDA mixture was cured in a similar manner for 3 hours at 150°C to form isotropic, amorphous thermoset films.

After these initial base cures, the NaCl plates were dissolved and the films floated off the glass slide in a distilled water bath, yielding homogenous, free-standing films of approximately 30 μm in thickness. The free-standing films were picked up on coarse size copper grids (1.0 mm × 1.0 mm), as shown in Fig. 4. The grids had been previously annealed in a vacuum at 800°C for 1 hr and coated in a dilute solution of DGEBA/MDA in tetrahydrofuran. The films were then bonded firmly to the grids with an additional post- cure of 180°C for 1 hour. This post-cure was also employed in order to devitrify the network and attain the maximum degree of cure [40]. The absence of the epoxide group was verified in [14] by observing the infrared absorption peak at 918 cm^{-1} which is due to the asymmetric stretch of the oxirane ring.

2.3. Mechanical testing

The samples were mounted in a motorized (Motomatic Electrocraft Corp, Model E552-S) straining stage with

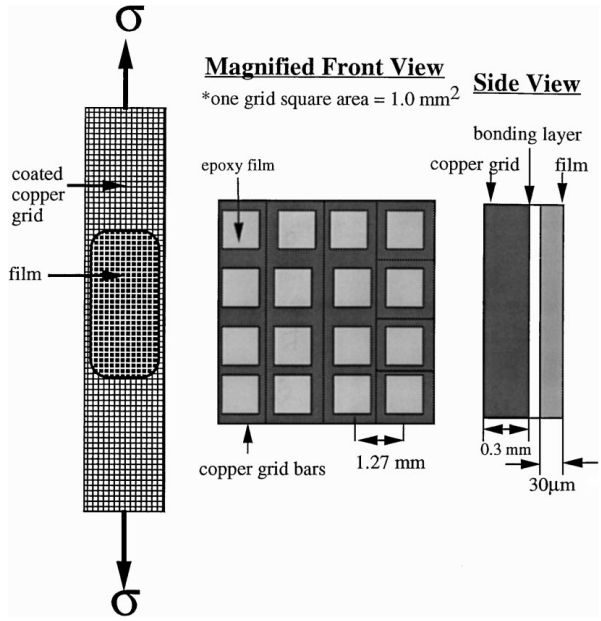

Figure 4 Schematic of sample preparation for microdeformation experiments; bonding of thermoset thin films 30 μm in thickness to annealed copper grids.

an initial gauge length, L_0, of one inch and strained at a displacement rate of 0.0025 in/s. Deformation and fracture mechanisms were observed under the polarized optical microscope with the straining axis at an angle of 45° to the polarizer or analyzer axis. Quantitative fracture analysis was accomplished by recording the number of grids squares with microcracks nucleated and the number of grid squares completely failed (i.e. with microcracks extending across the entire grid square) versus the displacement, δ. These values were then converted into the percentage of grid squares deformed, $P(\%)$, versus engineering strain, $\varepsilon_n = \Delta L / L_0$. The critical engineering strain for microcrack nucleation and propagation, ε_c was measured at $P = 50\%$.

3. Results and discussion

3.1. Isotropic, amorphous thermoset

The microdeformation and fracture of densely crosslinked epoxy-based, amorphous thermoset (network

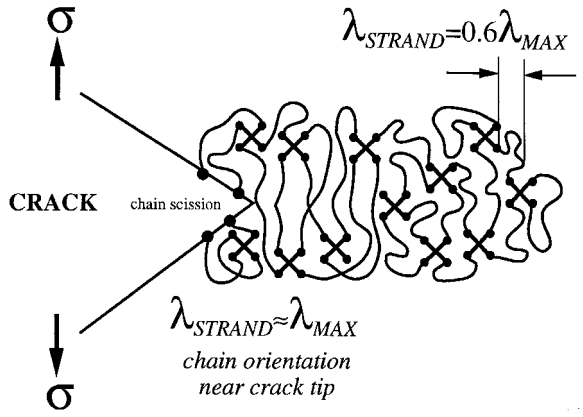

Figure 5 Schematic of fracture on a molecular scale in non-LC, amorphous, densely crosslinked thermosets; cracks are formed and propagate by the chain scission of covalent bonds.

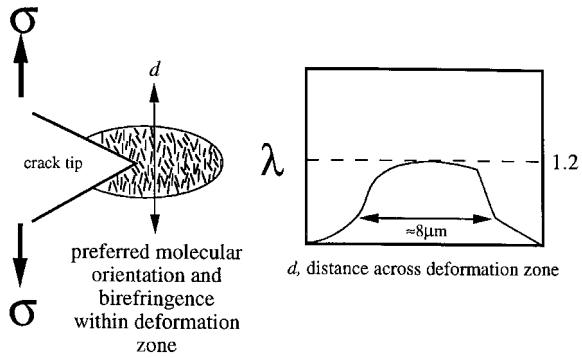

Figure 6 Schematic of the microdeformation mechanisms of non-LC, amorphous, densely crosslinked thermosets; microcracks form with diffues plastic deformation zones ahead of the crack tip [27].

strand density, $\nu_X \approx 10^{27}$ strands/m^3, or $\sim$1 monomer between crosslinks) thin films in tension is a topic which was studied extensively by Glad [27]. At low strains, microcracks nucleate from local stress-concentrators such as microscopic inhomogeneities in the film, density fluctuations, etc. On the smallest scale, the polymer chains directly in front of the crack tip are highly extended and eventually crack propagation occurs by scission of covalent bonds (Fig. 5). On a slightly larger scale, diffuse shear plastic deformation zones (DZ's) of approximately 8 μm in length exist just ahead of the crack tip (Fig. 6), as opposed to crazes which are observed in more loosely crosslinked polymer networks ($\nu_X < 4 \times 10^{25}$ strands/m^3 [32, 35]). These plastic deformation zones are regions in which the molecular strands have a preferred orientation parallel to the tensile axis and an extension ratio of $\lambda \approx 1.2$. The DZ's become reduced in width, more localized, and highly strained as the network strand density is reduced [27] (Fig. 7). In such thin films, the DZ is the primary energy dissipating mechanism at the crack tip and hence, controls the fracture toughness. DZ's are related to the phenomenon of strain softening, i.e. the post-yield drop in true stress with increasing true strain in a uniaxial compression test.

On the largest scale (i.e. a single grid square), the following observations were made on the 30 μm DGEBA/MDA thin films (Fig. 8). Since the material is initially isotropic, the films appear dark between crossed-polars. At small strains, the films exhibit a slight birefringence due to a combination of small amounts of local chain orientation along the stress axis, i.e. the photoelastic effect [41], and possibly tipping of the phenyl rings. At a critical strain, a single microcrack

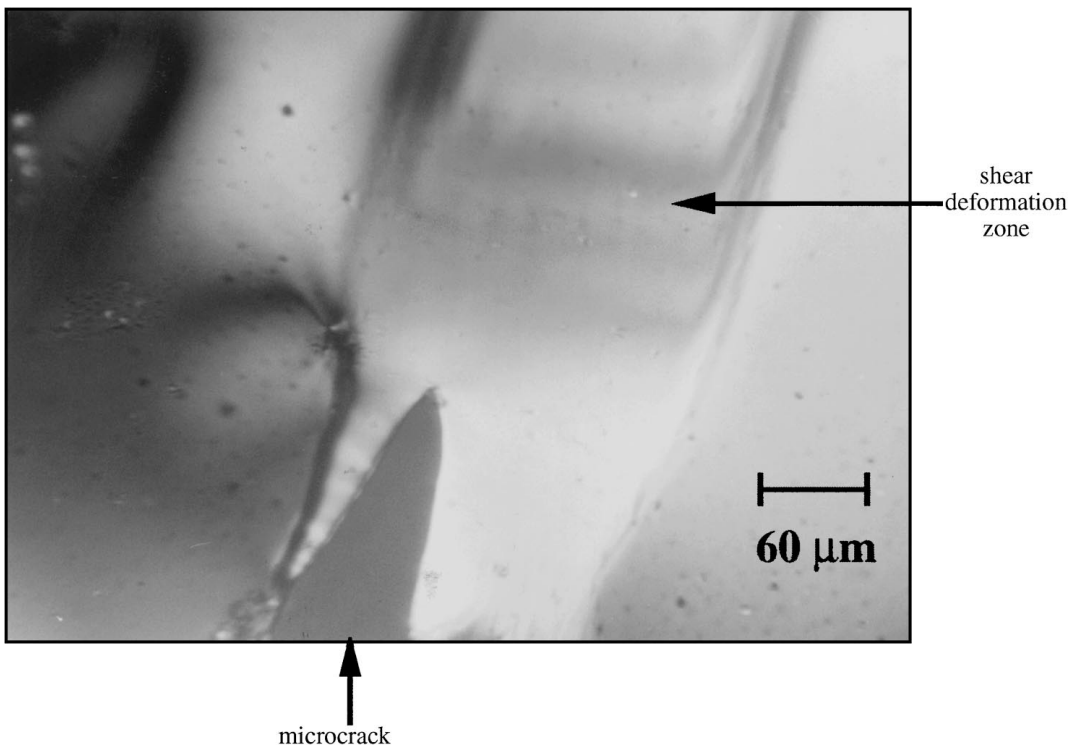

Figure 7 Microcrack and shear deformation zone in DGEBA/MDA non-LC, amorphous thermoset thin film (starting epoxy monomer molecular weight, $M_E = 1650$ g/mol) strained in tension under the polarizing optical microscope.

nucleates with a greater degree of birefringence around the crack tip than in the surrounding film due to the local stress concentration. This process leads to unstable, rapid crack propagation perpendicular to the strain axis and results in immediate and catastrophic, brittle fracture of the films. Upon failure, all of the birefringence is lost (even along the crack fronts and at the crack tip), indicating that the deformation was primarily elastic. The crack fronts appear straight and the rest of the film featureless and undeformed. This behavior is completely analogous to the bulk fracture of amorphous thermosets. Hence, even though there is a small, diffuse plastic deformation zone ahead of the crack tip (as found by Glad [27]), it does not dissipate enough energy to suppress catastrophic, brittle failure and subsequently leads to very low fracture toughness in these materials.

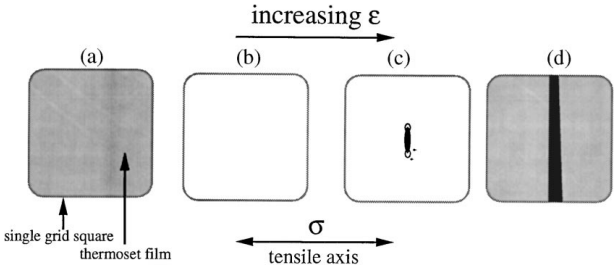

Figure 8 Qualitative fracture mechanisms of amorphous, densely crosslinked thermoset thin films as viewed under the polarizing optical microscope with increasing strain; (a) film appears dark with no birefringence, $\Delta n = 0$, because it is isotropic, (b) the photoelastic effect is observed with a corresponding slight increase in birefringence, $\Delta n \neq 0$, (c) a single microcrack nucleates with a larger amount of birefringence ahead of the crack tip, and (d) unstable, brittle, catastrophic failure, rapid crack propagation and complete loss of all Δn.

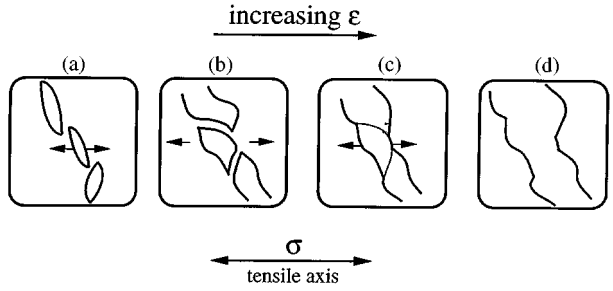

Figure 9 Qualitative fracture mechanisms of smectic LCT thin films as viewed under the polarizing optical microscope with increasing strain; (a) nucleation of multiple microcracks, (b) slow growth of microcracks and widening of crack tip opening displacements, (c) microcrack interconnection, and (d) complete film failure.

3.2. Smectic LCT

The microdeformation and fracture mechanisms of the smectic LCT were found to be very different than that of the amorphous thermoset and are summarized schematically in Fig. 9. At low strains, an increased birefringence was observed to take place homogeneously within the LC domains, i.e. there is little or no change in the Schlieren texture. Soon after, the nucleation of multiple diamond-shaped microcracks occurs, each oriented differently with respect to the straining axis. On the smallest scale, one can see numerous smaller isolated and interconnected defects (of the order of a single domain, $\sim$1 μm) surrounding and emanating from the crack tip (Figs 10 and 11). There is no evidence for localized plastic deformation zones, increased birefringence (greater than the elastic birefringence), or any changes in the Schlieren texture near the crack tip. With increasing strain, the microcracks propagate slowly and stably and exhibit large crack opening displacements of the crack tips, which are in most cases rounded and blunt. These observations are indicative of homogeneous, large-scale plastic deformation and consistent with the results on bulk fracture measurements of ref. [14]. At a critical size of $\sim$250 μm (Fig. 12), the cracks stop propagating, begin to open up laterally (along the stress axis), and change direction, leading to curved and jagged crack fronts (Fig. 13). At high strains, the cracks interconnect leading to complete film failure (Fig. 14) at which time all of the strain-induced birefringence is lost. Similar observations were also reported recently by Sue *et al*. [1] on smectic LCT thin films investigated by transmission electron microscopy.

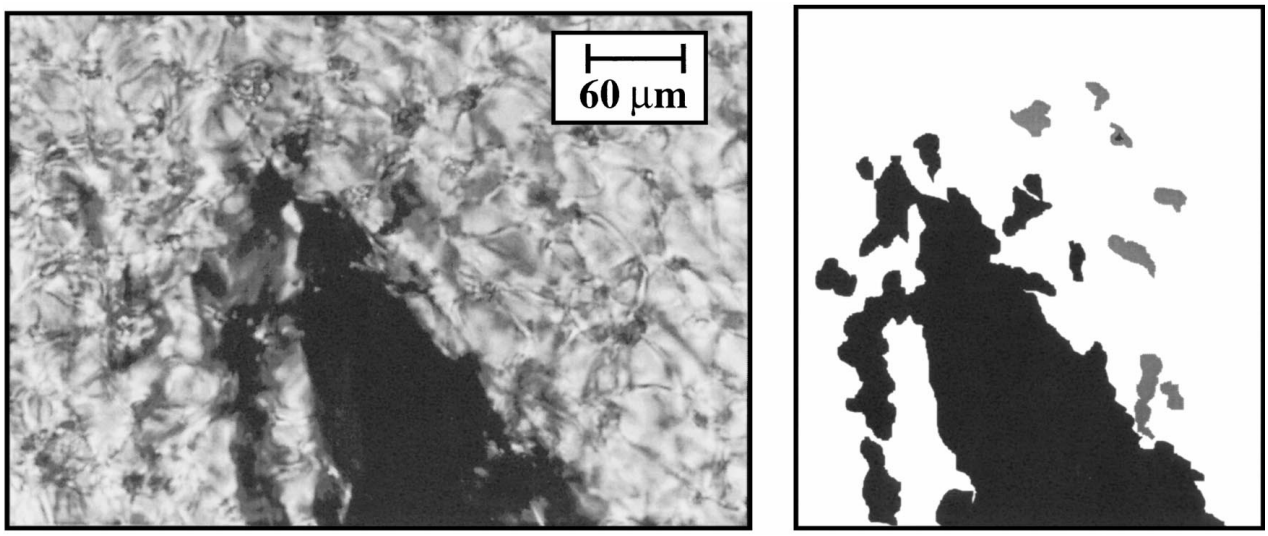

Figure 10 Large microcrack and smaller microcracks in DGDHMS/ MDA polydomain, smectic LCT thin film strained in tension under the polarizing optical microscope.

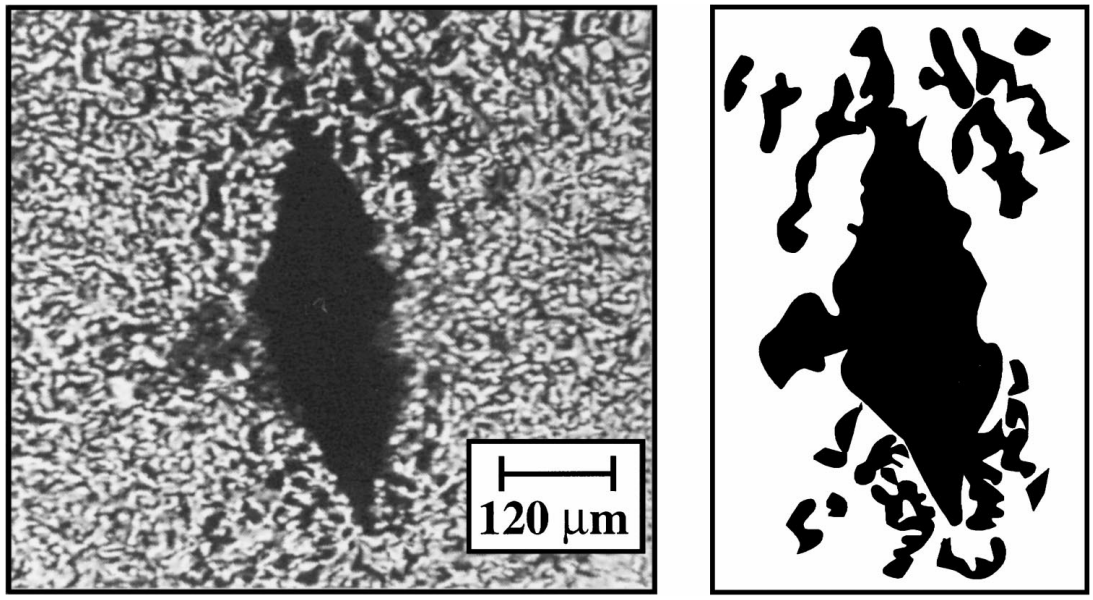

Figure 11 Large microcrack in DGDHMS/MDA polydomain, smectic LCT thin film strained in tension under the polarizing optical microscope.

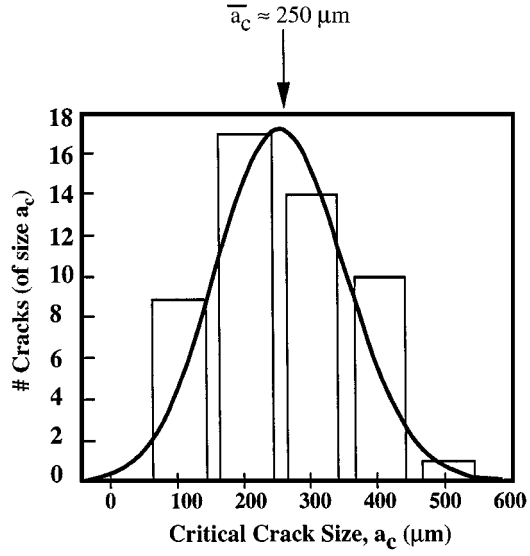

Figure 12 Distribution of microcrack sizes prior to changing crack propagation direction.

The microdeformation and fracture behavior observed for the smectic LCT's can be discussed in relation to the true stress versus true strain curve in uniaxial compression (Fig. 15) [14]. The lack of well-developed plane stress deformation zones and inhomogeneous yielding may be associated with the absence of a strain softening regime in the bulk uniaxial compression test. This is not a disadvantage in this case because instead of catastrophic, brittle failure taking place, homogeneous, bulk plastic deformation occurs leading to higher fracture toughness. There may be a number of possible reasons for the lack of the localized plastic deformation zones in the smectic LCT. Recent work on a loosely crosslinked (∼50 monomers between crosslinks) main-chain, smectic LC elastomer [42] suggests that mechanical deformation takes place by reorientation and rotation of the molecules within single LC domains along the strain axis, i.e. the disclinations remain intact upon deformation and even become more pronounced, sharper domain walls. Most likely, this is also the case for the smectic LCT (of course, to a much lesser degree due to the high crosslink density and decreased mobility of the network strands) and hence, it would be extremely difficult, if not impossible, to form a homogeneous region of molecular orientation ahead of the crack tip of ∼8 μm when the typical LC domain size is <1 μm. Instead, the domains prefer to fail in an individual and isolated manner. These are most likely the microscopic defects which appear in front of and around the crack tip (Figs 10 and 11). The networks strands of unfavorable oriented domains (perpendicular or nearly perpendicular to the stress direction) should be "softer" [43] and fail first, thus producing a series of microscopic voids ahead of the crack tip and around the crack. Neighboring domains can then deform under uniaxial rather than triaxial stress and undergo significant plastic deformation, similar to the deformation processes in rubber-modified thermosets [44] and polycrystalline metals [45]. Microcrack interconnection probably leads to the macroscopically fibrillar fracture surfaces observed under the SEM in bulk fracture toughness experiments (Fig. 2b).

3.3. Quantative analysis

Quantitative analysis of the amorphous thermoset gives a critical engineering strain for microcrack nucleation, $\varepsilon_{c(\text{nucleation})}$, equal to the critical strain for microcrack failure, $\varepsilon_{c(\text{failure})}$, of ≈20%. The lack of incubation time between nucleation and failure was also observed by Glad [20] on much thinner (∼0.5 μm) thermoset films of the same material. The smectic LCT (Fig. 16) exhibited a lower critical strain for microcrack nucleation, $\varepsilon_{c(\text{nucleation})} \approx 10\%$, and a critical strain for microcrack failure, $\varepsilon_{c(\text{failure})} \approx 14\%$, giving a 4% delay between nucleation and failure.

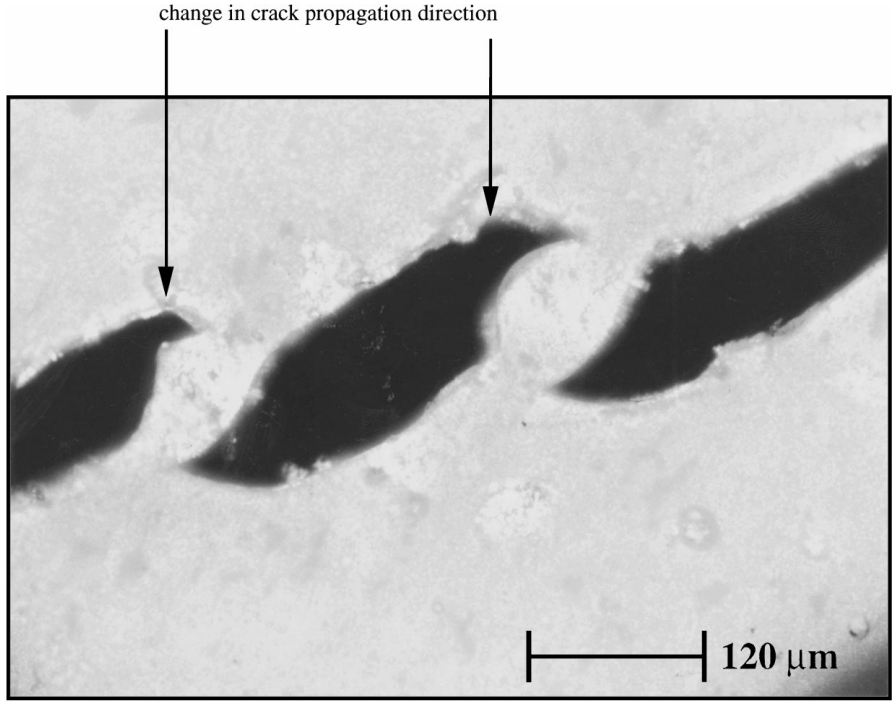

Figure 13 Multiple microcracks in DGDHMS/MDA smectic, polydomain LCT thin film strained in tension under the polarizing optical microscope.

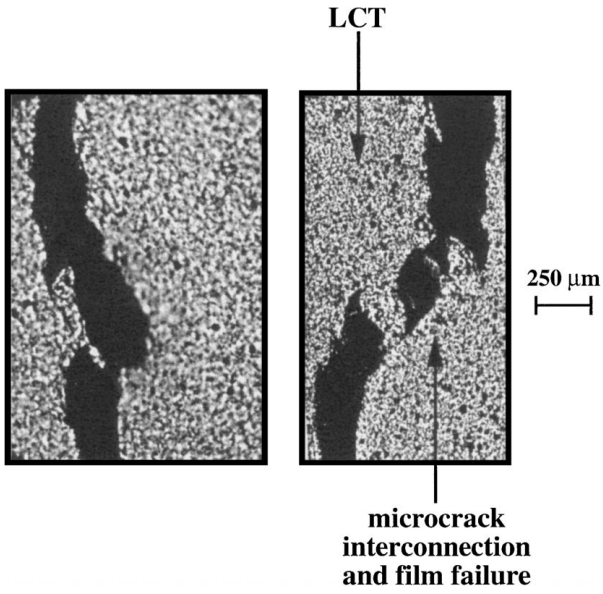

Figure 14 Microcrack interconnection in DGDHMS/MDA smectic, polydomain LCT thin films strained in tension under the polarizing optical microscope.

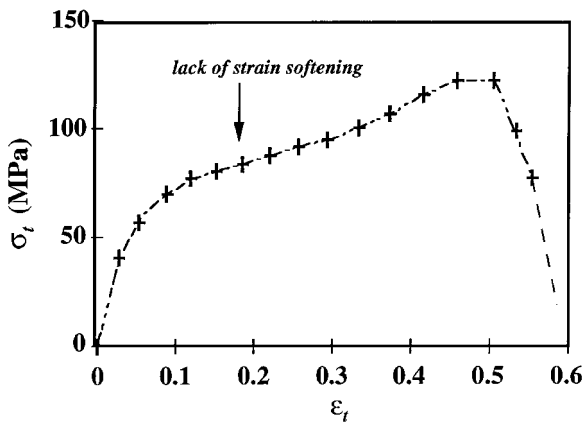

Figure 15 True stress versus true strain for DGDHMS/MDA smectic, polydomain LCT in uniaxial compression [14].

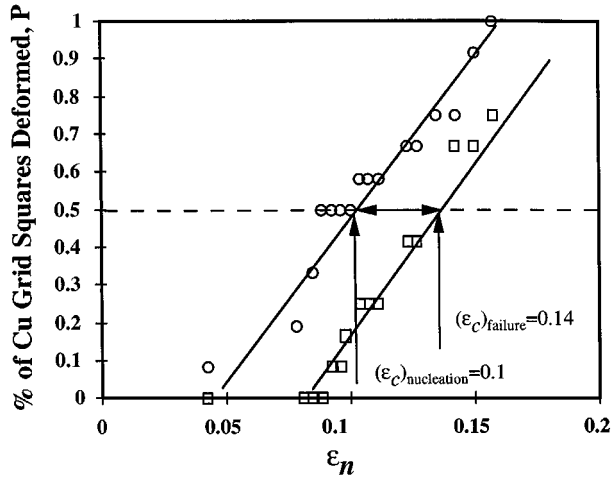

Figure 16 Quantitative microdeformation of DGDHMS/MDA smectic, polydomain LCT thin film strained in tension; (○) nucleation of microcracks and (□) film failure.

4. Conclusions

1. *Amorphous thermoset*. The amorphous, non-LC thermoset films exhibited brittle, catastrophic failure through the formation of a single microcrack which propagated perpendicular to the strain axis. The diffuse shear plastic deformation zones found by Glad [17] to be present ahead of the crack tip were unable to dissipate enough energy in order to suppress this type of failure mechanism and hence, this is why these materials exhibit a low fracture toughness.

2. *Smectic LCT*. A new type of microdeformation and fracture mechanism was observed for smectic LCT thin films involving the nucleation, slow propagation, branching, and eventual interconnection of numerous microcracks. There was no evidence of localized plastic deformation zones (greater than the size of a single LC domain $\sim 1\ \mu$m) or changes in the polydomain, Schlieren texture, even near the crack tip. Instead, the

LC domains prefer to fail in an individual and isolated manner, thus forming microscopic defects in front of and around the crack tip. These "voids" most likely relieve triaxial stresses and enable significant plastic deformation within neighboring domains, leading to a very high fracture toughness.

Acknowledgements

The authors would like to acknowledge the following people who assisted in polymer synthesis; Jia Shiun-Lin, Audrey Robinson, Dr. Yakhov Freidzon, Dr. Allen Gabor, Dr. Scott Clingman, Dr. Guo Ping Mao, and Dr. Hilmar Koerner. For technical consultation we would also like to thank Dr. Hilmar Koerner, Atsushi Shiota, and Maura Weathers (X-ray diffraction experiments and analysis), Margaret Rich (optical microscopy), and George Chevalier (mechanical testing). This research was sponsored by the National Consortium for Graduate Degrees for Minorities in Science and Engineering (GEM, Inc.), The Department of Education (DOE), and the National Science Foundation (NSF).

References

1. H.-J. SUE, J. D. EARLS and R. E. HEFNER, JR., in Proceedings of the 10th Annual International Conference of the Institute of Materials; Deformation, Yield, and Fracture of Polymers, Churchill College, Cambridge, UK, April 7–10th, 1997, (Chameleon Press Ltd, 1997) p. 129.
2. M. LAUS, R. PERNOZZOLI, H. KOERNER and C. K. OBER, in XII convegno italiano di scienza e tecnologia delle macromolecole, Palermo, Italy, 1995, p. 661.
3. J. D. EARLS and R. E. HEFNER, JR., European Patent Appl. #0-379-057A2, assigned to the Dow Chemical Company, 1990.
4. S. JAHROMI, W. A. G. KUIPERS, B. NORDER and W. J. MIJS, *Macromolecules* **28** (1995) 2201.
5. R. A. M. HIKMET and D. J. BROER, *Polymer* **32** (1991) 1627.
6. C. CARFAGNA, E. AMENDOLA and M. GIAMBERINI, *Composite Struct.* **127** (1994) 37–43.
7. *Idem.*, in Proceedings of the International Workshop on Liquid Crystalline Polymers, Capri, Italy, June 1–4, 1993, edited by C. Carfagna (Pergamon Press, Oxford, UK, 1994) p. 69.
8. W.-F. A. SU, *J. Polym. Sci.: Part A: Polym. Chem.* **31** (1993) 3251–3256.
9. A. SHIOTA and C. K. OBER, *J. Polym. Sci.: Polym. Phys. Ed.* **36** (1998) 31–38.
10. M. H. LITT, W.-T. WHANG, K.-T. YEN and X.-J. QIAN, *J. Polym. Sci: Part A: Polym. Chem.* **31** (1993) 183–191.
11. A. P. MELISSARIS and M. H. LITT, *Macromolecules* **127** (1994) 2675–2684.
12. A. P. MELISSARIS, J. K. SUTTER, M. H. LITT, D. H. SCHEIMAN and M. SCHEIMAN, *ibid.* **128** (1995) 860–865.
13. G. G. BARCLAY, S. G. MCNAMEE, C. K. OBER, K. I. PAPATHOMAS and D. W. WANG, *J. Polym. Sci.: Part A: Polym. Chem.* **30** (1992) 1843–1853.
14. C. ORTIZ, R. KIM, E. RODIGHIERO, C. K. OBER and E. J. KRAMER, *Macromolecules* **31**(13) (1998) 4074–4088.
15. G. BARCLAY, S. G. MCNAMEE, C. K. OBER, K. I. PAPATHOMAS and D. W. WANG, *J. Polym. Sci.: Part A: Polym. Chem.* **30** (1992) 1831–1843.
16. P. G. DE GENNES, "The Physics of Liquid Crystals," (Claredon Press, Oxford, 1974).
17. W. H. DE JEU, "Physical Properties of Liquid Crystalline Materials," (Gordon and Breach Scientific Publishers, 1980).
18. D. DEMUS and L. RICHTER, "Textures of Liquid Crystals," (VCH Publications, 1978).
19. H. KELKER and R. HATZ, "Handbook of Liquid Crystals," (Verlag Chemie, 1980).
20. E. B. PRIESTLEY, P. J. WOJTOWICZ and P. SHENG (eds.), "Introduction to Liquid Crystals," (Plenum Press, 1974).
21. G. VERTOGEN and W. H. DE JEU, "Thermotropic Liquid Crystals: Fundamentals," (Springer-Verlag, 1988).
22. P. J. COLLINGS, "Liquid Crystals: Nature's Delicate Phase of Matter," (Princeton University Press, 1990).
23. A. M. DONALD and A. H. WINDLE, "Liquid Crystalline Polymers," (Cambridge University Press: Cambridge, UK, 1992).
24. R. A. GLEDHILL, A. J. KINLOCH, S. YAMINI and R. J. YOUNG, *Polymer* **19** (1978) 574.
25. G. PRITCHARD and G. V. RHODES, *Matls. Sci. Eng.* **28** (1976) 1.
26. R. J. YOUNG, "Developments in Polymer Fracture-1," edited by E. H. Andrews (Applied Science: London, 1979) Ch. 6.
27. M. D. GLAD, PhD thesis, Department of Materials Science and Engineering, Cornell University, Ithaca, N.Y., 1990.
28. B. D. LAUTERWASSER and E. J. KRAMER, *Phil. Mag.* **39A** (1979) 469.
29. G. WISANRAKKIT and J. K., *J. Appl. Polym. Sci.* **41** (1990) 2885–2929.
30. A. M. DONALD and E. J. KRAMER, *J. Matls. Sci.* **16** (1981) 2967–2976.
31. *Idem., ibid.* **16** (1981) 2977–2987.
32. *Idem., ibid.* **17** (1982) 1871–1879.
33. *Idem., J. Polym. Sci.: Polym. Phys. Ed.* **20** (1982) 899–909.
34. *Idem., Polymer* **23** (1982) 1183.
35. C. HENKEE and E. J. KRAMER, *J. Polym. Sci.: Polym. Phys. Ed.* **22** (1984) 721–737.
36. P. MILLER and E. J. KRAMER E. J., *J. Matls. Sci.* **25** (1990) 1751.
37. A. C.-M. YANG, *Matls. Chem. Phys.* **41** (1995) 295–298.
38. L. L. BERGER and E. J. KRAMER, *J. Matls. Sci.* **22** (1987) 2739–2750.
39. C. J. G. PLUMMER, J. L. HEDRICK, H.-H. KAUSCH and J. G. HILBORN, *J. Polym. Sci.: Part B Polym. Phys.* **33** (1995) 1813–1820.
40. G. WISANRAKKIT and J. K. GILLHAM, *J. Appl. Polym. Sci.* **41** (1990) 2885–2929.
41. M. M. LEVEN (ed.), "Photoelasticity," (Pergamon Press, 1941).
42. C. ORTIZ, M. WAGNER, N. BHARGAVA, C. K. OBER and E. J. KRAMER, *Macromolecules* **38** (1998) 8531–8539.
43. It has been shown that oriented polymers exhibit much lower moduli when strained perpendicular to the direction of orientation. (I. M. Ward (ed.), "Structure and Properties of Oriented Polymers," (Applied Science Publishers, Ltd.: London, 1975) Ch. 7.)
44. It is thought that the main toughening mechanism in rubber-modified thermosets comes from rubber particles which debond and cavitate under stress, thus generating a series of voids which can relieve triaxial stresses in the matrix and promote the energy-absorbing process of shear yielding. (Y. HUANG and A. J. KINLOCH, *Polymer* **33** (1992) 1330; F. J. GUILD and A. J. KINLOCH, *J. Mater. Sci.* **30** (1995) 1689.)
45. G. E. DIETER, JR., "Mechanical Metallurgy," (McGraw-Hill Book Company, Inc.: New York, 1961) p. 202.

Received 7 October 1997
and accepted 10 March 1999